Proc. R. Soc. Lond. A **424**, 263–278 (1989)
Printed in Great Britain

The quantum phase 2-form near degeneracies: two numerical studies

BY R. J. MONDRAGON AND M. V. BERRY, F.R.S.
H. H. Wills Physics Laboratory, Tyndall Avenue, Bristol BS8 1TL, U.K.

(*Received* 1 *February* 1989)

The phase of a quantum state changes rapidly as parameters $X = (X_1, X_2, \ldots)$ are varied near a degeneracy X^*, reflecting the monopole singularity of the underlying phase 2-form $V(X)$ at X^*. The singularities may be sources or sinks of V. We study them numerically and display them graphically for two families of hamiltonians whose degeneracy structure is typical. First is a particle moving along a line segment with kinetic energy quartic in the momentum ('quartic-momentum square well'); the X are incorporated into the boundary conditions. Second is a charged particle moving in a domain D of the plane which is threaded by a magnetic flux line of strength α, with wavefunction vanishing on the boundary ∂D ('Aharonov–Bohm billiards'); the X are α and parameters specifying ∂D; V is not invariant under gauge transformations of the vector potential generating the flux. For Aharonov–Bohm billiards we study how the spatial patterns of phase of wavefunctions change round circuits near degeneracies; these patterns also have singularities (wavefront dislocations) that appear and disappear by colliding with each other and with ∂D.

1. INTRODUCTION

Attention has recently been directed to the geometric phase γ acquired when a quantum state $|n(X)\rangle$ is driven round a cycle C in the space of parameters $X = (X_1, X_2 \ldots)$ on which it depends (Berry 1984, and other papers collected by Shapere & Wilczek 1989). A more fundamental quantity is the phase 2-form $V(X)$, whose flux through C gives γ.

$$\gamma = -\iint_{\partial S = \mathrm{C}} V(X). \tag{1}$$

In terms of the state $|n\rangle$,

$$V(X) = \mathrm{Im}\,\langle \mathrm{d}n| \wedge |\mathrm{d}n\rangle, \tag{2}$$

where d denotes differentiation in X space. If $|n\rangle$ is an eigenstate of a parameter-dependent hamiltonian $H(X)$, with eigenstate $E_n(X)$, then

$$V(X) = \mathrm{Im} \sum_{m \neq n} \frac{\langle n|\mathrm{d}H|m\rangle \wedge \langle m|\mathrm{d}H|n\rangle}{(E_n - E_m)^2}. \tag{3}$$

In this case the cycling of $|n\rangle$ can be effected by the adiabatic cycling of H. If there are three parameters, the wedge products in (2) and (3) can be written as a cross product of gradient vectors in X-space:

$$\mathrm{d}A \wedge \mathrm{d}B = \nabla_x A \wedge \nabla_x B \cdot \mathrm{d}\boldsymbol{S}, \tag{4}$$

where $\mathrm{d}\boldsymbol{S}$ is the vector area element. Then the 2-form can be written as a vector:

$$V = \boldsymbol{V}\cdot\mathrm{d}\boldsymbol{S}. \tag{5}$$

V (or $\boldsymbol{V}$) is a gauge field in parameter space, invariant under the transformation,

$$|n(X)\rangle \rightarrow |n(X)\rangle \exp\{\mathrm{i}\mu(X)\}, \tag{6}$$

for arbitrary $\mu(X)$. The singularities of V occur at degeneracies X^* involving the state $|n\rangle$, and are of monopole type, diverging as $|X\text{-}X^*|^{-2}$.

In this paper our main aim is to show by numerical calculation for two hamiltonians that V does have the predicted monopole form near degeneracies. The hamiltonians must be complex hermitian rather than real symmetric; otherwise V vanishes (cf. equation (3)). In physical terms this means there must be neither time-reversal symmetry (T) nor any other antiunitary symmetry (Robnik & Berry 1986) throughout X. There may, however, be surfaces in X where $H(X)$ has T, provided that symmetry is broken in a transverse direction, because then the components of V in the surface can be non-zero.

Degeneracies are harder to find in systems without T because (in the absence of any unitary symmetry, e.g. geometric) they have codimension 3, whereas with T they have codimension 2 (Von Neumann & Wigner 1929). The nearby phase structure is also richer: without T, γ is given (in suitable coordinates) by half the solid angle subtended by C at X^*, whereas with T the only possible phases are $\gamma = 0$ and $\gamma = \pi$. In this sense we are generalizing an earlier study (Berry & Wilkinson 1984) of degeneracies (diabolical points) in systems (triangle quantum billiards) with T.

Our subsidiary aim is to examine a different sort of phase singularity, namely dislocations in the spatial phase structure (Nye & Berry 1974) of quantum states in position representation, as the state is varied close to a degeneracy.

2. Quartic-momentum square well

This is a family of one-dimensional systems which we have studied before (Berry & Mondragon 1986), whose degeneracies have the codimension of the typical case, but which can be solved analytically. A quantum particle with wavefunction $\psi_n(x;X) = \langle x\,|\,n(X)\rangle$ moves on the interval $|x| \leqslant 1$. Its hamiltonian operator is defined by

$$H(X)\,\psi_n = \frac{\mathrm{d}^4\psi_n}{\mathrm{d}x^4} \equiv \psi_n'''' = E_n\,\psi_n \equiv k_n^4\,\psi_n \tag{7}$$

with parameters $X = (a, b, c, d)$ incorporated in the boundary conditions

$$\begin{bmatrix}\psi_n''(\pm 1)\\ \psi_n'''(\pm 1)\end{bmatrix} = \begin{bmatrix}c+\mathrm{i}d & \pm a\\ \pm b & -c+\mathrm{i}d\end{bmatrix}\begin{bmatrix}\psi_n(\pm 1)\\ \psi_n'(\pm 1)\end{bmatrix}. \tag{8}$$

When $d \neq 0$, H is complex; when $d = 0$, H is real.

For all X, H is symmetric about $x = 0$. Therefore the eigenstates have even or odd parity. Within each class the degeneracies all have $d = d^* = 0$. In the subspace a, b, c of real hamiltonians, degeneracies lie along infinite lines. The nth of these corresponds to degeneracies between the nth and $(n+1)$ st states, so that each state degenerates twice; once each with its upper and lower neighbours.

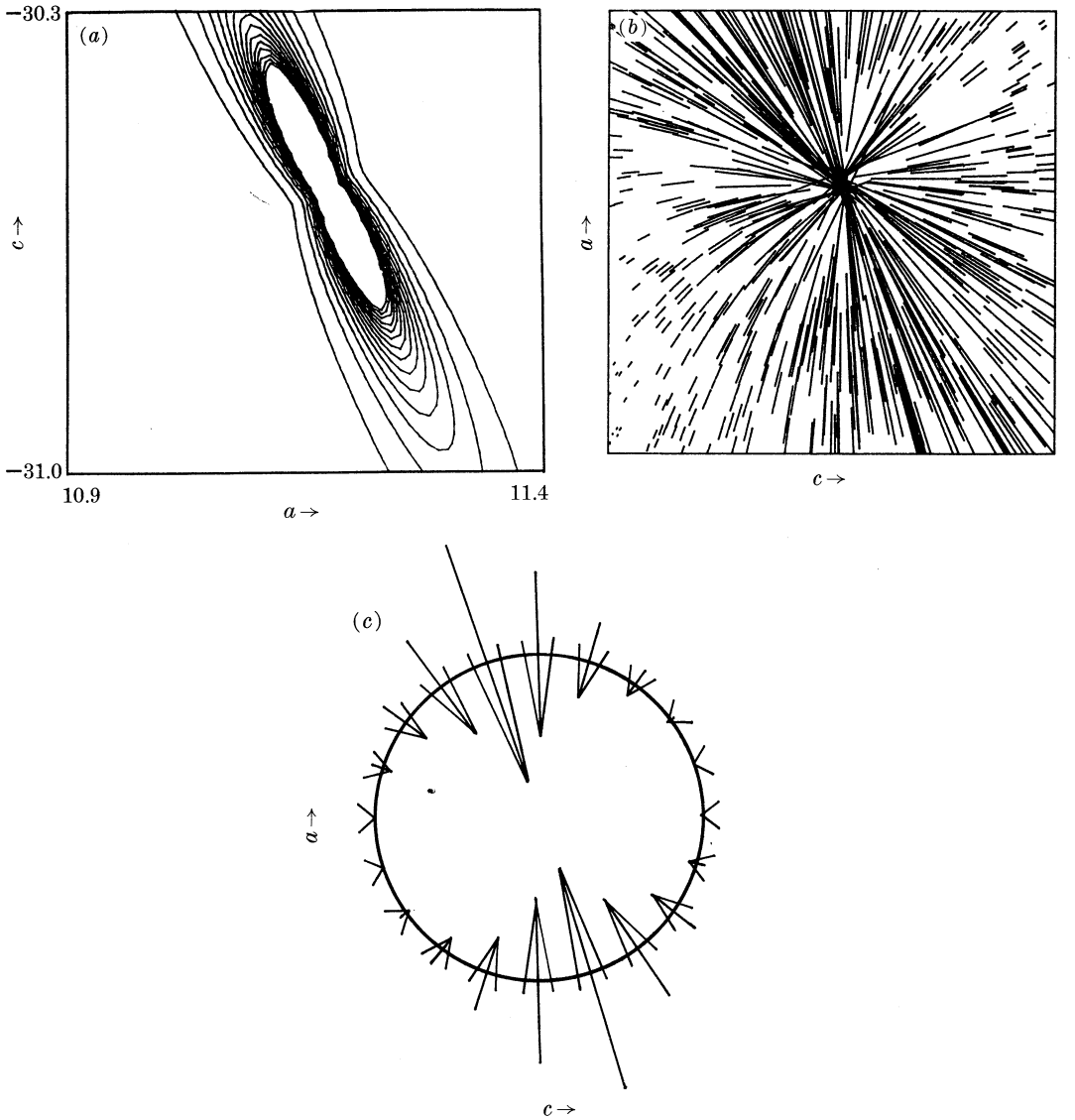

FIGURE 1. Phase 2-form V for the state $|2\rangle$ near its degeneracy with $|3\rangle$. for the quartic-momentum square well. The singularity has parameters $X^* = (a^*, b^*, c^*, d^*) = (11.2, 68.6, -30.6, 0)$ and energy $k^* = 6.8$. V lies in the subspace a, c with fixed $b = b^*$ and $d = 0$. (*a*) Contours of $|V|$; (*b*) lines of V; (*c*) directions of V on a circuit surrounding X^*.

Thus the degeneracies have the typical codimensions: 3 in the full space of hermitian hamiltonians and 2 in the subspace of real ones.

Here we work only with the even states

$$\psi(x; X) = N(\mu \cos kx + \nu \cosh kx), \tag{9}$$

where the coefficients μ, ν, the normalization constant N and the eigenvalue k all depend on a, b, c, d. Thus V can be evaluated directly from the definition (2).

As there are four parameters we can fix one arbitrarily (we choose $b = 68.6$)

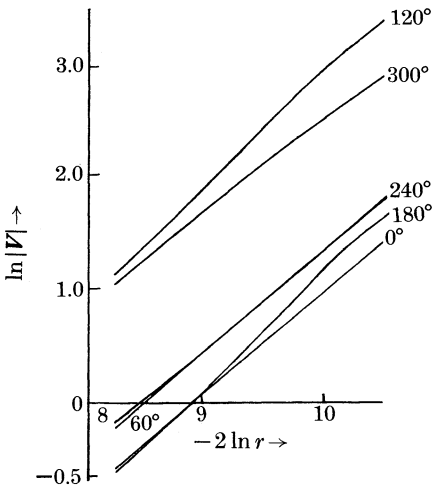

FIGURE 2. Monopole character of the singularity in figure 1, demonstrated by the unit slope of the doubly logarithmic plot of $|V|$ against r^{-2} where $r = [(a-a^*)^2+(c-c^*)^2]^{\frac{1}{2}}$ is distance from X^* in the subspace $b = b^*$, $d = 0$. The lines represent approaches to X^* along the indicated directions.

and study the phase 2-form as a vector $\boldsymbol{V}$ in the space of the other three (a, c, d). When $d = d^* = 0$, H is real, so that (cf. (2) and (4)) $\boldsymbol{V}$ has no d component; it lies entirely in the plane a, c containing the degeneracies.

Figure 1 shows $\boldsymbol{V}$ in the a, c-plane for the state $|2\rangle$ near its degeneracy with $|3\rangle$. The singularity is obvious, and figure 1 *c* shows that it is a sink rather than a source. Figure 2 shows that the singularity has the expected monopole divergence.

Figure 3 is a wider view that also shows the other degeneracy involving $|2\rangle$, namely that with $|1\rangle$. This degeneracy is a source of $\boldsymbol{V}$.

3. Aharonov–Bohm billiards

3.1. *Hamiltonian*

A quantum charged particle moves in a domain D of the plane $\boldsymbol{r} = (x, y)$, and is reflected specularly at the boundary ∂D. Threading D at $\boldsymbol{r} = 0$ is a single line of magnetic flux of strength α (in quantum units). The parameters X are those specifying the form of ∂D, together with α. Wavefunctions $\psi_n(r; \boldsymbol{X}) = \langle \boldsymbol{r}|n(X)\rangle$ are governed by the hamiltonian

$$\left.\begin{aligned} H\psi_n = -[\nabla_r - \mathrm{i}\boldsymbol{A}(\boldsymbol{r};X)]^2\psi_n = E_n\psi_n \quad &\text{in D,} \\ \psi_n = 0 \quad &\text{on } \partial\text{D,} \end{aligned}\right\} \tag{10}$$

where the vector potential $\boldsymbol{A}$ satisfies

$$\nabla_r \wedge \boldsymbol{A} = 2\pi\alpha\delta(\boldsymbol{r}). \tag{11}$$

It is the magnetic flux that breaks T and makes H complex hermitian rather than real symmetric.

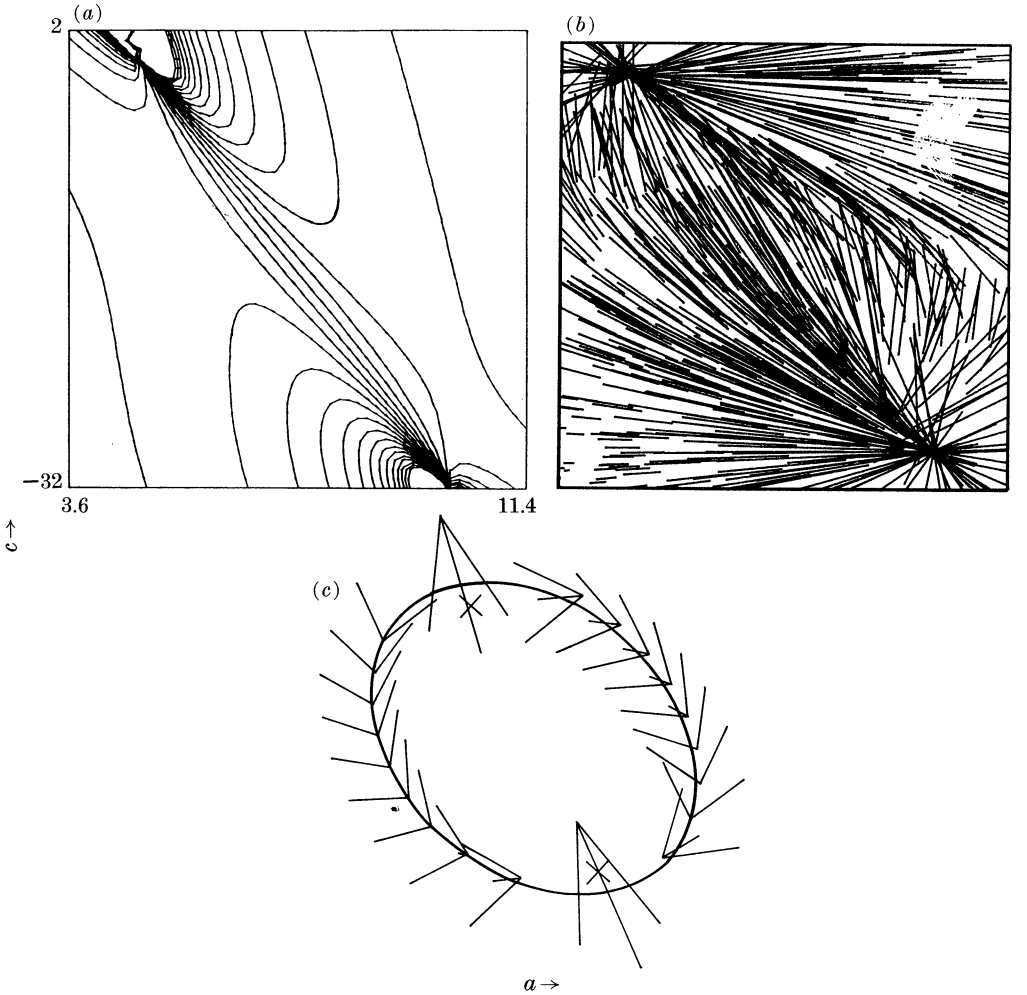

FIGURE 3. As figure 1 but also showing the degeneracy between $|2\rangle$ and $|1\rangle$, at $X^* = (3.7, 68.6, 1.17, 0)$ and $k^* = 4.0$.

The hamiltonian (10) and (11) was introduced by Berry & Robnik (1986*a*) as a model for quantum chaology (Berry 1987) in the absence of T. Their technique for diagonalizing H was based on the conformal transformation of D to the unit disk (an Aharonov–Bohm billiard which can be solved exactly). It works best if the transformation is a low-order polynomial. The lowest order for which ∂D has no geometric symmetry is 3, which generates the boundary,

$$x + \mathrm{i}y = \mathrm{e}^{\mathrm{i}\theta} + B\,\mathrm{e}^{2\mathrm{i}\theta} + C\,\mathrm{e}^{(3\mathrm{i}\theta+\phi)} \quad (0 \leqslant \theta < 2\pi), \tag{12}$$

parametrized by B, C, ϕ. The domain of allowed values of B, C is bounded by the requirement that ∂D must not self-intersect. We fix $\phi = \frac{1}{3}\pi$, so our H has the 3 parameters $X = (B, C, \alpha)$. The conformal method for solving quantum billiards was devised by Robnik (1984) who applied it to the case without flux (i.e. with T) and $C = 0$ (heart-shaped billiards, with reflection symmetry).

The vector potential $\boldsymbol{A}$ must satisfy (11), but this still leaves it undetermined by the addition of the gradient of a single-valued scalar function. We resolve this gauge freedom by choosing $\boldsymbol{A}$ in a way that makes conformal calculations easiest; parallel to ∂D at the boundary. Then $\boldsymbol{A}$ is the velocity field of fluid swirling irrotationally in D down a plughole at $\boldsymbol{r} = 0$. It is a surprising fact, first noted in a related context by Aharonov & Anandan (1987), that the quantum phase 2-form V (equation (2)) is not invariant under parameter-dependent magnetic gauge transformations. If $\boldsymbol{A}$ is changed to

$$\boldsymbol{A}'(\boldsymbol{r}; X) = \boldsymbol{A}(\boldsymbol{r}; X) + \nabla_r \Lambda(\boldsymbol{r}; X), \tag{13}$$

V transforms to

$$V'(X) = V(X) + \mathrm{d} \wedge \langle n|\mathrm{d}\Lambda|n\rangle. \tag{14}$$

This result is derived, and its physical significance explained, in Appendix A. Of course V is still invariant under the gauge transformation (6), which is of a different type.

3.2. *Degeneracies and phase 2-form*

When the magnetic flux α is non-zero, degeneracies for the non-symmetric billiards (B and C both non-zero) have codimension 3 so all parameters $X = (B, C, \alpha)$ must be explored. For each X, a matrix must be diagonalized. This makes the search for these degeneracies very time-consuming, so we looked only at the lowest 15 levels. We found 10 degeneracies. Symmetries reduce the codimension and thereby make the search simpler. We found 49 degeneracies associated with symmetry. The existence of each degeneracy was confirmed by checking the monopole divergence of the 2-form (cf. figure 2).

Two levels can degenerate more than once. Figure 4 shows an example when $\alpha = 0$, that is for the non-magnetic billiard. The degeneracies involve states $|7\rangle$ and $|8\rangle$. The elliptic contours of the level separation show the conical structure recognized by Teller (1937).

In computing the 2-form we used the sum-over-states (3) rather than the simpler-looking formula (2), because it was easier to calculate derivatives of H (in terms of derivatives of the matrix generated by the conformal technique) than to define a continuation for the state $|n\rangle$ and compute its derivatives; moreover each diagonalization automatically produced the extra states $|m\rangle$ needed to evaluate (3). In no case were more than 30 states required in each evaluation of (3) to ensure convergence of V to the accuracy shown in the figures to follow. Even so, calculations of V were slow because to calculate the nth level with an error less than 5% of the mean spacing required the diagonalization of a $5n \times 5n$ (complex) matrix.

Figure 5 shows two examples of V near a degeneracy. In 5*a–c* the degeneracy is the right-hand one in figure 4, so H is real symmetric. In 5*d–f* the degeneracy (involving states $|14\rangle$ and $|15\rangle$) has non-zero α so H is complex hermitian.

Figure 6 is a wider view of figure 5*a–c* which also shows the other degeneracy in figure 4. In contrast to figure 3, which also shows two degeneracies, both degeneracies involve the same two states and their monopoles are both sources of V.

Each of the figures 5 and 6 took about 70 hours of CPU time on a VAX730 computer.

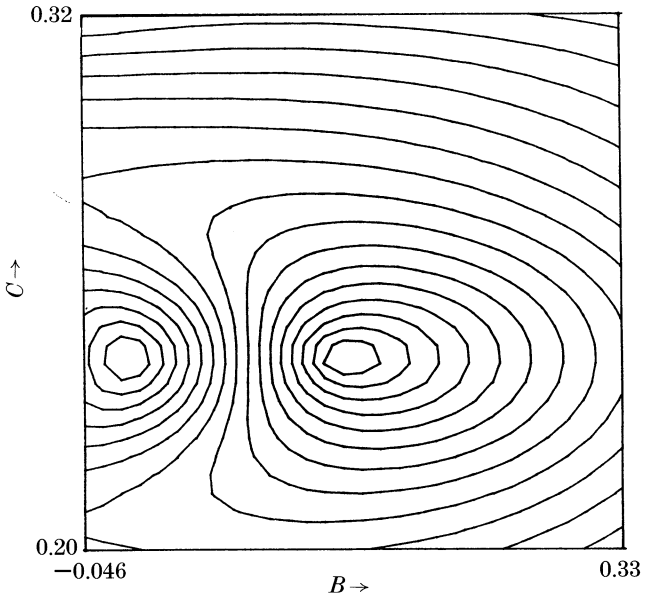

FIGURE 4. Contours of level separation $E_8(B,C)-E_7(B,C)$ for quantum billiards with $\alpha = 0$, showing degeneracies at $X^* = (B^*, C^*, \alpha^*) = (0, 0.227, 0)$ and $(0.204, 0.242, 0)$. The loops near the degeneracies are ellipses.

3.3. *Phase dislocations in wavefronts*

Here we study the phase of quantum billiard wavefunctions $\psi_n(\boldsymbol{r};X)$ as a function of position $\boldsymbol{r} = (x, y)$, as X makes a cycle C near a degeneracy X^*.

When H is real (e.g. when there is T), ψ_n is real as well and so its only phases are 0 and π. Phase structure is then embodied in the nodal lines, which divide D into nodal cells. Because a degeneracy has codimension 2, it can be enclosed by C, around which nodal cells must change sign. When C is small we can write either of the degenerating states as

$$\psi_n(\boldsymbol{r};\, X(\theta)) = \cos(\tfrac{1}{2}\theta)\,\psi_{\mathrm{A}}(r) + \sin(\tfrac{1}{2}\theta)\,\psi_{\mathrm{B}}(\boldsymbol{r}) \quad (0 \leqslant \theta \leqslant 2\pi), \tag{15}$$

where θ is an angle parametrizing C and ψ_{A} and ψ_{B} are two degenerate states at X^*.

The way the nodal patterns change with θ has been illustrated for the (integrable) square billiard (Korsch 1983) and for (non-integrable) triangle billiards (Berry & Wilkinson 1984). Here we show in figure 7 the states during the rightmost degeneracy in figure 4. As with the other examples, the rearrangement of nodal cells (black into white) is accomplished not simply by sliding round within D but by topological changes involving crossing of nodal lines (at $\theta \approx 95°$ and $\theta \approx 103°$).

When H is complex, the phase structure is much richer. Writing

$$\psi_n(\boldsymbol{r};X) \equiv \rho(\boldsymbol{r};X)\exp\{\mathrm{i}\chi(\boldsymbol{r};X)\}, \tag{16}$$

we see that the phase structure is embodied in the *wavefronts* $\chi = \text{const.} \times \mathrm{mod}\, 2\pi$. These form a pattern with singularities at the nodal points $\rho = 0$ (where χ is

FIGURE 5. For description see opposite.

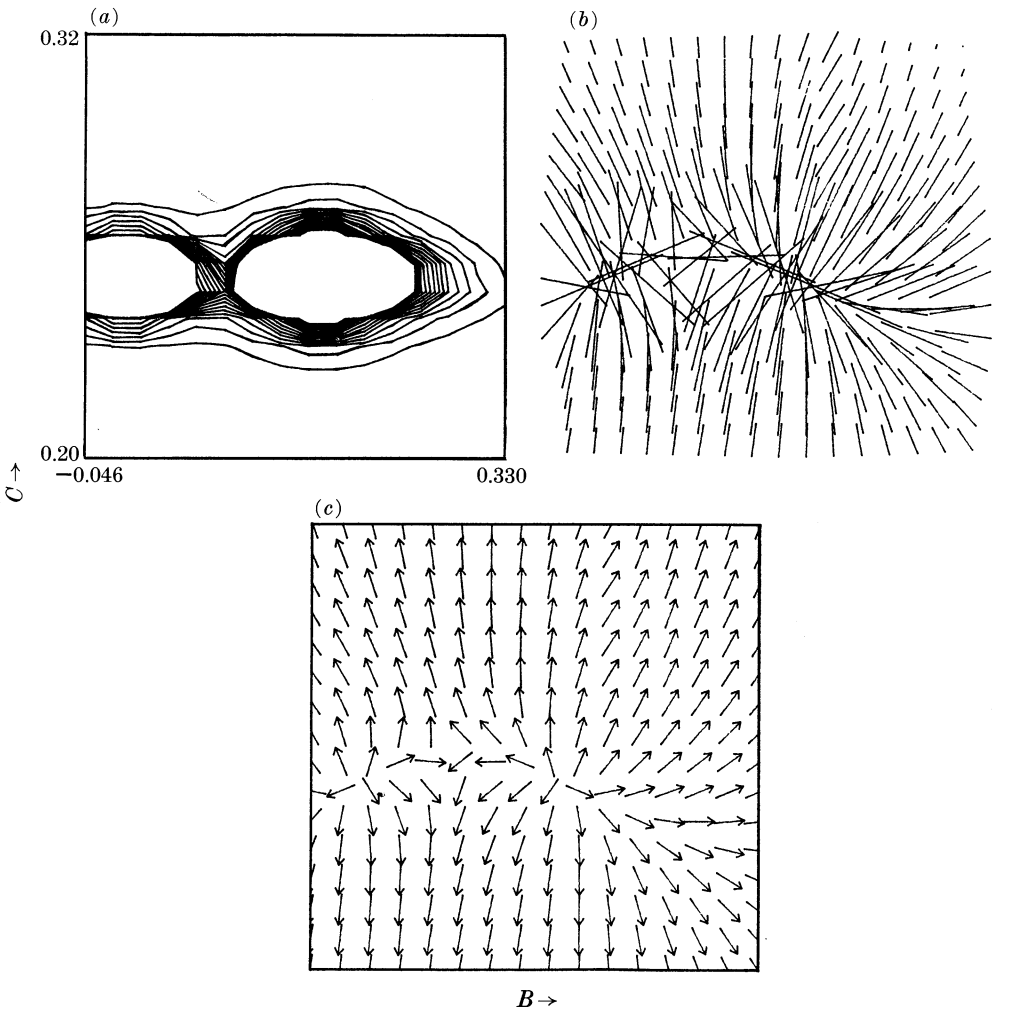

FIGURE 6. As figure 5*a–c* but showing both degeneracies in figure 4.

undefined). The singularities are called *phase dislocations* (Nye & Berry 1974, see also Berry 1981). Dislocations in Aharonov–Bohm billiards were studied by Berry & Robnik (1986*b*) for fixed ∂D and varying flux α.

Here we fix α at a degenerate value α^* and study the wavefronts as ∂D, determined by parameters B, C in (12), is cycled round the degeneracy between states $|14\rangle$ and $|15\rangle$, for which the 2-form is shown in figure 5*d–f*. Figure 8 shows

FIGURE 5. (*a*)–(*c*) Phase 2-form V for the state $|7\rangle$ near its degeneracy with $|8\rangle$, for the quantum billiard (12) in the plane $\alpha = 0$. The singularity is at $X^* = (B^*, C^*, \alpha^*) = (0.204, 0.242, 0)$. In this subspace, H is real symmetric, so V lies in the BC-plane. (*a*) Contours of $|V|$; (*b*) lines of V; (*c*) directions of V on a circuit surrounding X^*. (d)–(f) As (a)–(c) but for the state $|14\rangle$ near its degeneracy with $|15\rangle$, for the Aharonov–Bohm billiard in the plane $\alpha = 0.382$; the degeneracy is at $X^* = (B^*, C^*, \alpha^*) = (0.309, 0.223, 0.382)$; in (*e*) V is shown projected onto the BC-plane, with the heavy line showing where the component along α changes sign.

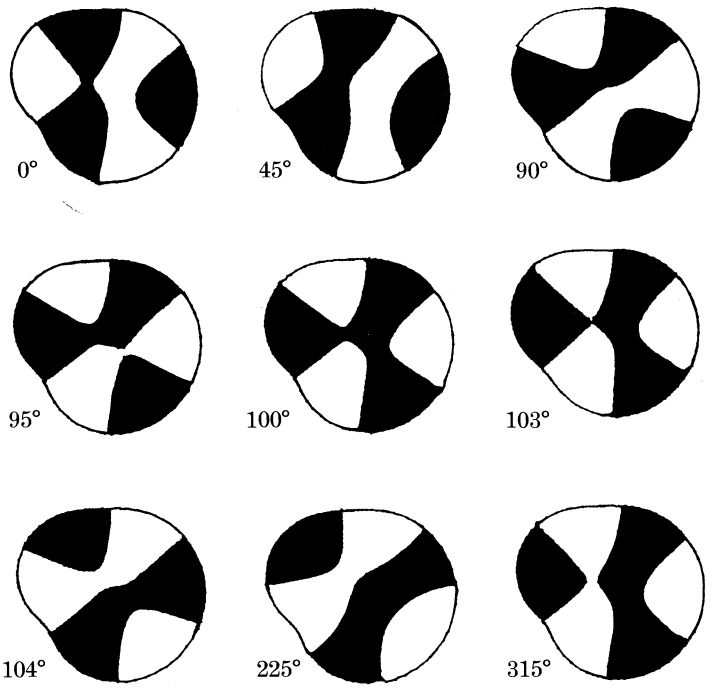

FIGURE 7. Rearrangement of nodal cells around the degeneracy between states $|7\rangle$ and $|8\rangle$ of the quantum billiard (12), at $X^* = (B^*, C^*, \alpha^*) = (0.204, 0.242, 0)$. The labels give the values of the mixing angle in (15).

an overview of the phase patterns round the cycle. The wavefronts are not labelled by their phase values because these depend on the phase continuation rule used to transport the state; under the parallel-transport rule the labellings of the wavefronts at the beginning and end of C would differ by the geometric phase γ (here π because C lies in a plane including X^*). Note that wavefronts meet the boundary perpendicularly (unless χ has a saddle there); this was explained by Berry & Robnik (1986*b*) as a consequence of choosing the gauge in which $\boldsymbol{A}$ is parallel to ∂D.

It is clear from figure 8 that the phase pattern and its changes round C are complicated. Dislocations can appear and disappear in two ways, illustrated in figures 9 and 10 and now described.

The first way is by annihilation and creation of pairs within D. Such an event conserves the dislocation strength in a circuit (in $\boldsymbol{r}$-space) surrounding it. Dislocation strength is an integer, defined as the total phase change of the wavefunction round the circuit, divided by 2π. Individual dislocations almost always have strength ± 1. If the circuit is ∂D, the total dislocation strength S of the billiard is given by the boundary integral

$$S(X) = \frac{1}{2\pi}\int_0^1 \mathrm{d}\tau \frac{\mathrm{d}}{\mathrm{d}\tau} \operatorname{Im} \ln \{\boldsymbol{n}(\tau)\cdot\nabla_r \psi_n(\boldsymbol{r}(\tau); X)\}, \tag{17}$$

where $0 \leqslant \tau < 1$ parametrizes ∂D and $\boldsymbol{n}$ is the normal to ∂D at τ.

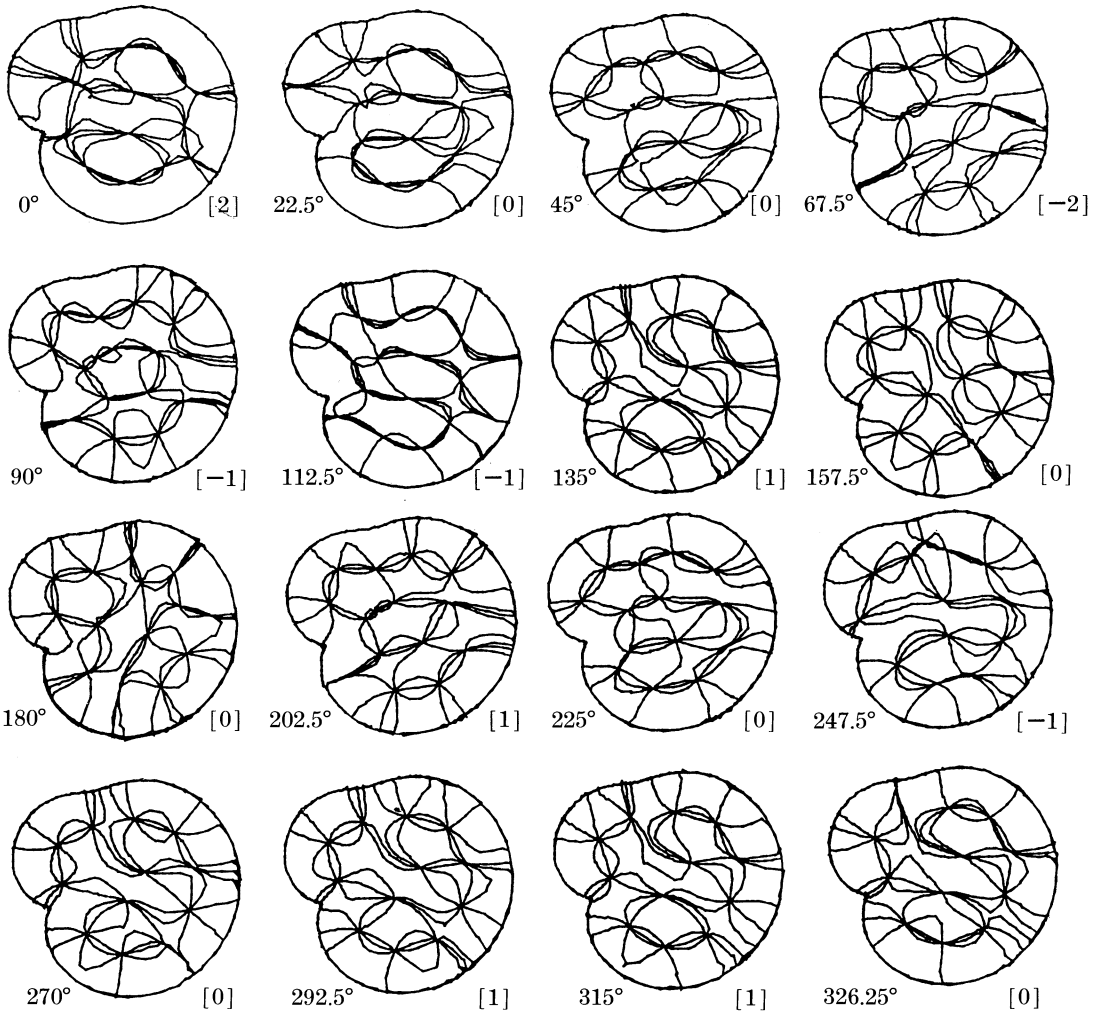

FIGURE 8. Pattern of wavefronts around the degeneracy at $X^* = (B^*, C^*, \alpha^*) = (0.309, 0.223, 0.382)$ between states $|14\rangle$ and $|15\rangle$. C is a circle in BC-space with radius 10^{-3}, centred on B^*, C^* and parametrized by the angle shown in the pictures; α is fixed at α^*. The numbers in square brackets give the dislocation strength defined by (17). Wavefronts are shown at intervals of $\frac{1}{4}\pi$.

Figure 9 is a magnification of the part of C that includes the last two pictures in figure 8. Two dislocations are created near 337.5°; one of these annihilates with a third near 356.25°. A more detailed view of these processes is shown in figure 10*a*. Similar events have been discussed in connection with acoustic piston radiators (Wright & Berry 1984) and ocean tide waves (Nye *et al.* 1988).

The second way of making dislocations appear is for two to be created on ∂D and then move off it, one inside D and the other outside. Of course the process can also occur in reverse. Creations and annihilations of this type cause S to change by ± 1. It is not possible for a single dislocation to migrate across ∂D because in that process the wavefronts could not remain perpendicular to ∂D as they must. Nye

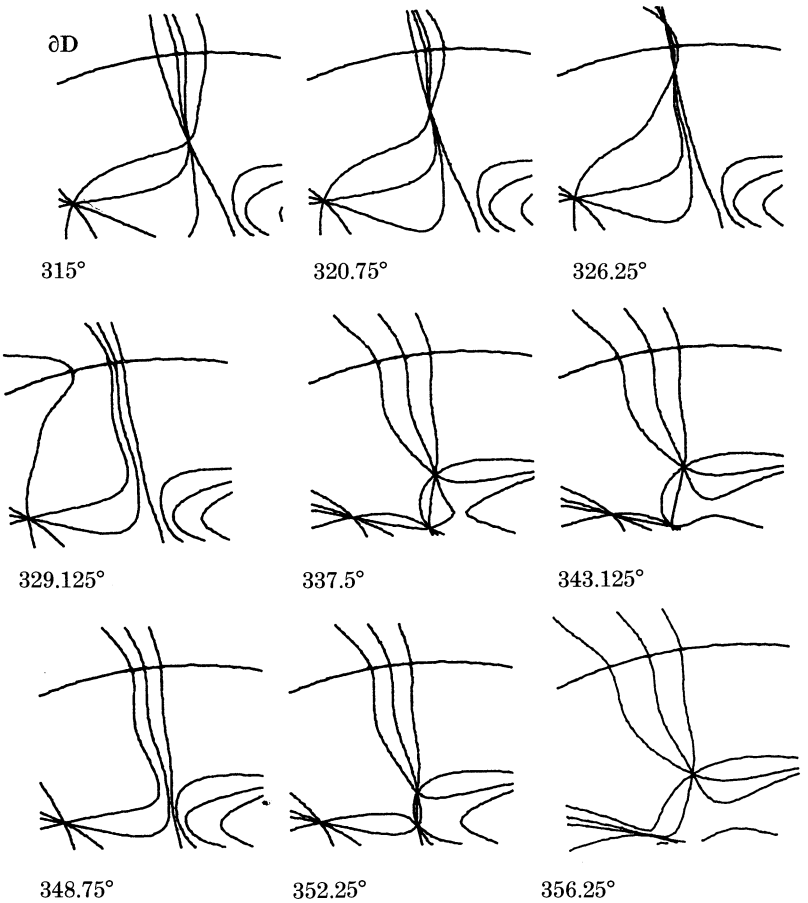

FIGURE 9. More detailed view of the sequence of wavefront patterns including the upper part of the last two pictures in figure 8. Two dislocations appear inside D near 337.5°; two dislocations annihilate inside D near 356.25°; two dislocations disappear on ∂D near 326.25°.

et al. (1988) give an elegant topological argument showing that the birth of a pair of dislocations must be accompanied by the birth of a pair of saddles of the phase function χ (only then are both dislocation strength and singularity index conserved). In the present problem the saddles separate along ∂D after the creation event.

Figure 9 shows that two dislocations annihilate on the boundary near 326.25°. The more detailed view in figure 10*b* also shows the associated boundary saddles (dotted).

We thank Dr J. H. Hannay for helpful discussions. R.J.M. thanks CONACYT (Mexico) and the H. H. Wills Physics Laboratory for support.

Appendix A. Change in phase 2-form under magnetic gauge transformation

As a result of the transformation (13) the wavefunctions, which are the solutions of (10), transform to

$$\psi'_n(\boldsymbol{r}; X) = \psi_n(\boldsymbol{r}; X)\exp\{\mathrm{i}\Lambda(\boldsymbol{r}; X)\}. \tag{A 1}$$

This superficially resembles (6), but here the phase factor occurs only in position representation rather than multiplying the Hilbert space vector representing the state. Thus the phase 2-form (2) transforms to

$$\begin{aligned} V'(X) &= \mathrm{Im}\iint \mathrm{d}\boldsymbol{r}\,\mathrm{d}\psi'^{*}_n \wedge \mathrm{d}\psi'_n \\ &= \mathrm{Im}\iint \mathrm{d}\boldsymbol{r}\,(\mathrm{d}\psi^{*}_n - \mathrm{i}\psi^{*}_n\,\mathrm{d}\Lambda)\wedge(\mathrm{d}\psi_n + \mathrm{i}\psi_n\,\mathrm{d}\Lambda) \\ &= V(X) + \mathrm{Re}\iint \mathrm{d}\boldsymbol{r}\,(\psi_n\,\mathrm{d}\psi^{*}_n + \psi^{*}_n\,\mathrm{d}\psi_n)\wedge\mathrm{d}\Lambda \\ &= V(X) + \iint \mathrm{d}\boldsymbol{r}\,\mathrm{d}|\psi_n|^2\wedge\mathrm{d}\Lambda \\ &= V(X) + \mathrm{d}\wedge\iint \mathrm{d}\boldsymbol{r}|\psi_n|^2\,\mathrm{d}\Lambda, \end{aligned} \tag{A 2}$$

which is the result (14).

The reason why the 2-form, and hence the geometric phase γ, is changed by the transformation generated by $\Lambda(\boldsymbol{r}; X)$ is that the parameters X depend on time, so that Λ generates an electric field through its rate of change and so can be expected to produce physical effects. These can be eliminated by completing the gauge transformation and allowing Λ to affect the scalar potential $U(\boldsymbol{r}; X)$ (in (10) U describes the infinitely hard wall at ∂D). The transformation is

$$U'(\boldsymbol{r};X) = U(\boldsymbol{r};X) - \frac{\mathrm{d}}{\mathrm{d}t}\Lambda(\boldsymbol{r};X) = U - \frac{\mathrm{d}X_i}{\mathrm{d}t}\frac{\partial\Lambda}{\partial X_i}. \tag{A 3}$$

The complete gauge transformation (13) and (A 3) has no effect on the total phase change γ_{tot} produced by cycling X, because its effect on the time-dependent wavefunction is to introduce the same phase factor as in (A 1) (whether the change in X is adiabatic or not) and this is single-valued in a cycle of X. But the change in the scalar potential U changes both the instantaneous eigenstates $|n(X)\rangle$ and the energies $E_n(X)$. Thus both the geometric and dynamic phases will change, and the changes must compensate.

We calculate the change in the dynamical phase γ_{d} from

$$\gamma'_{\mathrm{d}} = -\int_0^T \mathrm{d}t\,E'_n(X), \tag{A 4}$$

where T is the duration of the cycle. In the adiabatic limit T is large, so the

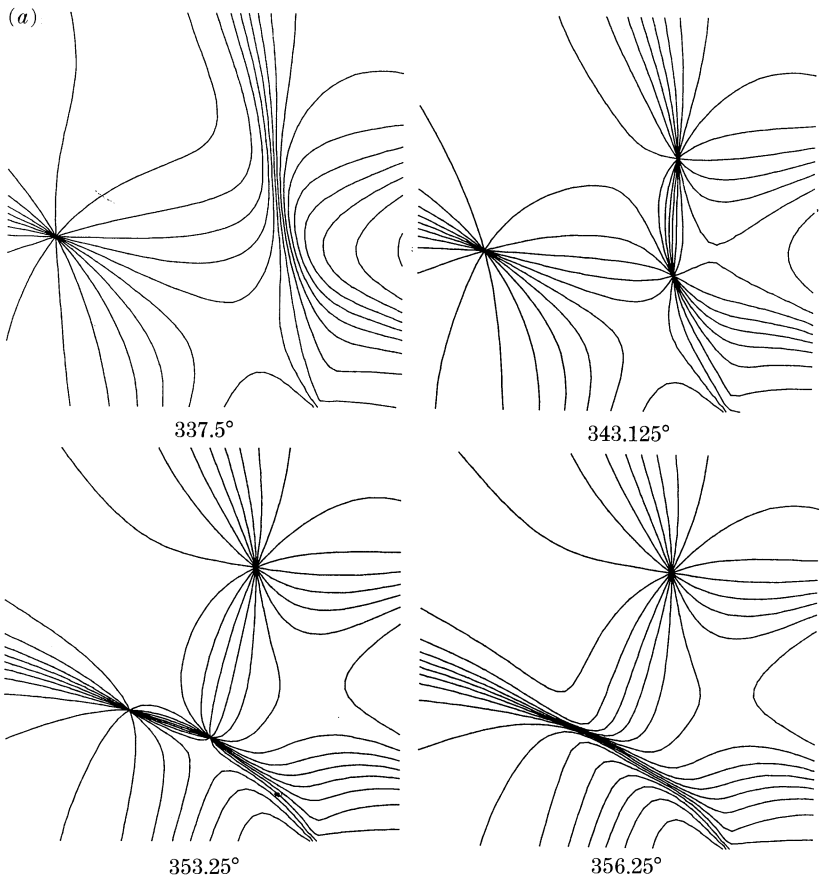

FIGURE 10*a*. For legend see opposite.

parameters change slowly and the effect on the energies of the gauge term in (A 3) can be evaluated by perturbation theory:

$$\gamma'_{\mathrm{d}} = -\int_0^T \mathrm{d}t\left(E_n - \frac{\mathrm{d}X_i}{\mathrm{d}t}\int\int \mathrm{d}\boldsymbol{r}\,\frac{\partial \Lambda}{\partial X_i}|\psi_n|^2\right) = \gamma_{\mathrm{d}} + \oint_{\mathrm{c}} \langle n|\mathrm{d}\Lambda|n\rangle. \tag{A 5}$$

The change in the geometric phase is obtained from (14) and (1):

$$\gamma' = \gamma - \int\int \mathrm{d}\wedge\langle n|\mathrm{d}\Lambda|n\rangle = \gamma - \oint_{\mathrm{c}} \langle n|\mathrm{d}\Lambda|n\rangle. \tag{A 6}$$

This shows that the changes do indeed compensate.

Because of the lack of magnetic gauge-invariance of the 2-form, there is some arbitrariness in the division of the phase change γ_{tot} into geometric and dynamic parts. Of course this does not destroy the physical significance of the geometric phase, which must always be included unless a special (*post hoc*) choice of magnetic gauge is made. Aharonov & Anandan (1987) discuss this gauge dependence of

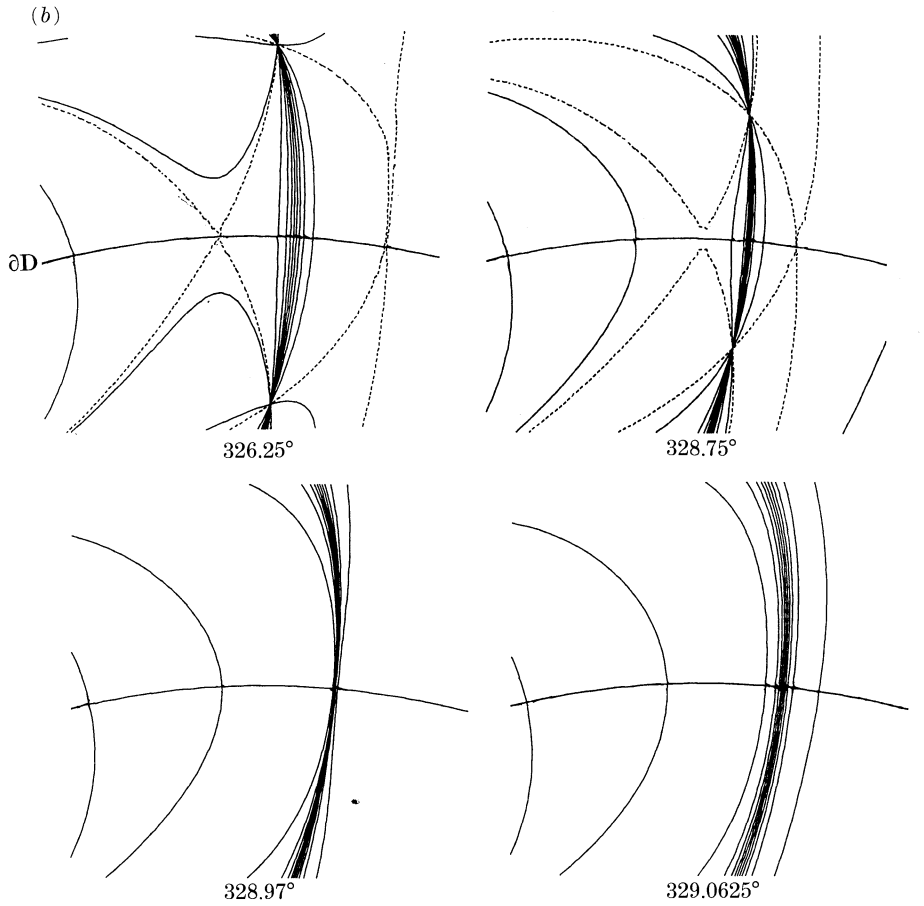

FIGURE 10. More detailed views of the events in figure 9, with wavefront interval $\frac{1}{10}\pi$; (*a*) inside D; (*b*) on ∂D.

γ in the general non-adiabatic case. They propose a redefinition of γ that would make it invariant under magnetic gauge transformations, by adding a term

$$-\int_0^T \mathrm{d}t\langle n(X(t))|U(\boldsymbol{r};\, X(t))|n(X(t))\rangle. \tag{A 7}$$

This proposal has the disadvantage that it prevents γ being written as an integral (line or surface) in parameter space, so that the geometric phase is no longer geometric, at least in the sense we mean here.

REFERENCES

Aharonov, Y. & Anandan, J. 1987 *Phys. Rev. Lett.* **58**, 1593–1596.

Berry, M. V. 1981 In *Physics of defects, Les Houches Lectures*, vol. 34 (ed. R. Balian, M. Kléman & J. P. Poirier), pp. 453–543. Amsterdam: North-Holland.

Berry, M. V. 1984 *Proc. R. Soc. Lond.* A **392**, 45–57.
Berry, M. V. 1987 *Proc. R. Soc. Lond.* A **413**, 183–198.
Berry, M. V. & Mondragon, R. J. 1986 *J. Phys.* A **19**, 873–885.
Berry, M. V. & Robnik, M. 1986*a* *J. Phys.* A **19**, 649–668.
Berry, M. V. & Robnik, M. 1986*b* *J. Phys.* A **19**, 1365–1372.
Berry, M. V. & Wilkinson, M. 1984 *Proc. R. Soc. Lond.* A **392**, 15–43.
Korsch, H. J. 1983 *Phys. Lett.* A **97**, 77–80.
Nye, J. F. & Berry, M. V. 1974 *Proc. R. Soc. Lond.* A **336**, 165–190.
Nye, J. F., Hajnal, J. V. & Hannay, J. H. 1988 *Proc. R. Soc. Lond.* A **417**, 7–20.
Robnik, M. 1984 *J. Phys.* A **17**, 1049–1074.
Robnik, M. & Berry, M. V. 1986 *J. Phys.* A **19**, 669–682.
Shapere, A. & Wilczek, F. (eds) 1989 *Geometric phases in physics.* Singapore: World Scientific.
Teller, E. 1937 *J. phys. Chem.* **41**, 109–116.
Von Neumann, J. & Wigner, E. 1929 *Phys. Z.* **30**, 467–470.
Wright, F. J. & Berry, M. V. 1984 *J. acoust. Soc. Am.* **75**, 733–748.